



Multi-objective optimization of process variables for MWCNT-added electro-discharge machining of 316L steel

Md Al-Amin¹ · Ahmad Majdi Abdul-Rani¹ · Rasel Ahmed² · Muhammad Umair Shahid³ · Fatema Tuj Zohura⁴ · Muhammad Danial Bin Abd Rani⁵

Received: 3 December 2020 / Accepted: 27 April 2021 / Published online: 5 May 2021
© The Author(s), under exclusive licence to Springer-Verlag London Ltd., part of Springer Nature 2021

Abstract

Fabrication of 316L steel with the desired surface integrity and thin modified recast layer for manufacturing various devices is very challenging using the traditional techniques and requires post-processing. Nevertheless, electro-discharge machining (EDM) is an evolving candidate among the non-traditional processes offering concurrent machining and surface alteration for the instrument manufacturing industry. To explore its full potential, this research work provides a thorough investigation of process variables on the machining performances and surface features primarily required for processing 316L steel in the industry. In this study, nano multi-walled carbon nanotubes (MWCNT) are utilized to improve the machining and surface responses. In addition to this, the parametric optimization is conducted through a Taguchi-based design which assists to obtain the highest material removal rate (MRR) of 42.25 mg/min corresponding to a 10-A peak current, 16- μ s pulse-on time, 1-g/l MWCNT amount, and 45% duty cycle while the lowest surface roughness (SR) and recast layer thickness (RLT) of 1.58 μ m and 5.243 μ m respectively are attained at a 5-A peak current, 8- μ s pulse-on time, 0.7-g/l MWCNT amount, and 45% duty cycle. Analysis of variance (ANOVA) reports peak current being the most momentous parameter complied by the MWCNT amount, pulse-on time, and duty cycle for MRR, SR, and RLT. The best 21 solution sets predicted through the multi-objective optimization tool called non-dominated sorting genetic algorithm-II (NSGA-II) obeying the set objective functions are proposed which are obtained from the Pareto optimal frontiers. Accuracy levels of the predicted solution sets are verified by the confirmatory experiments showing the estimated errors of less than 10%. SEM analyses confirm excellent surface integrity with a comparatively thin recast layer formation.

Keywords 316L steel · MWCNT · Electro-discharge · NSGA-II · Roughness · Material removal · Recast layer

1 Introduction

The 316L steel is commonly utilized in manufacturing medical implants, equipment of aerospace, power plants, and oil and gas industries since it attributes to low-cost, highly mechanical characteristics, biocompatibility, and resistance to corrosion [1, 2]. Through the traditional machining processes, such as turning CNC-milling, spinning, boring, CNC-lathe, shaping, the fabrication of 316L steel with complex shape geometry is very challenging due to the hard, ductile, and heat resistance features of it. The direct contact between the specimen and the tools may damage the surface machined because of wear and tear propagation caused by the relative movement of them. In addition to this, thermal stresses are developed in the part fabricated because of the uncontrolled heat generation caused by the friction and heat resistance characteristics of them. The particular cutting tools are required to machine a hard specimen such as 316L steel using

✉ Md Al-Amin
alamin0903091me@gmail.com

¹ Department of Mechanical Engineering, Universiti Teknologi PETRONAS, 32610 Bandar Seri Iskandar, Perak, Malaysia

² Department of Chemical Engineering, Universiti Teknologi PETRONAS, Bandar Seri Iskandar, Perak, Malaysia

³ Department of Materials Science and Engineering, Institute of Space Technology, Islamabad, Pakistan

⁴ Department of Agroforestry and Environment Science, Sher-e-Bangla Agricultural University, Sher-e-Bangla Nagar, Dhaka, Bangladesh

⁵ Lab Management Department, Universiti Teknologi PETRONAS, Bandar Seri Iskandar, Perak, Malaysia

the conventional techniques. Most notably, the conventional machining methods show low rate of material removal and high rate of cutting tool wear, resulting in low machining performance and an increase in production cost [3, 4]. Moreover, these processes cannot form a thin recast layer with moderate or nano-scale surface roughness. As a consequence, post-processing is required which increases the overall production expenditure [4, 5]. Electro-discharge machining (EDM) is an evolving non-traditional technique which enables concurrent machining and forming a recast layer on the machined component retaining a slight machining gap between the specimen and the tool electrode during the operation. Configuration and surface condition of the tool electrode employed influence shape and topography of the component machined. This method enables the fabrication of any conductive component with the complicated configuration regardless of the properties including stiffness, brittleness, and thickness of the material employed as the physical interactions between the specimen and the tool electrode do not exist. As a consequence, the EDM technique is successfully employed in manufacturing molds, dies, aerospace components, and medical equipment [6–10]. However, the stochastic nature and low machining performances including low MRR (material removal rate), high SR (surface roughness), and thick recast layer formation limit the EDM technique applications which lead to high machining cost with poor surface integrity [1, 4, 5, 9, 10].

The machining performances of EDM method including MRR, recast layer thickness (RLT), and SR depend on its process variables especially peak current, duty cycle, pulse-on time, applied voltage, and tool polarity. High application of the discharge energy in the plasma channel causes high material melting and removal from both the work part and the tool electrode leading to a rough machined surface with a thick recast layer formation [1, 3, 4]. Since a tiny operating gap between the work part and the tool electrode is maintained during the EDM process, unstable machining may occur due to insufficient flushing of the debris produced. The work part and the tool electrode come further close to create the plasma channel due to raising the electrical resistivity of them caused by a huge temperature formation during the conventional EDM process. As a consequence, a thick recast layer is formed on the surface machined which may cause mechanical malfunction of the instrument fabricated [11, 12]. In addition to this, the surface machined through the traditional EDM method attributes poor surface integrity with micro cracks and thermal stress formation because of a huge temperature ranging from 8000 to 12000 °C generation leading to the requirement of excessive heat removal from the machining zone. To overcome the aforesaid limitations, a novel process called powder-mixed EDM (PM-EDM) is introduced in which the electrically and thermally conductive nanoparticles are mixed in the working fluid to ameliorate the machining and surface responses [3, 4, 13]. The literatures have established that the addition of electrically conductive

powders including Cu, TiC, Al₂O₃, SiC, Al, Ti, Gr, and Si not only improve MRR but also deliver excellent surface integrity including a thin recast layer with the desired SR and less micro-crack formation because of ameliorating the flushing system caused by enlarging the machining gap, scouring effects of the debris eroded, and ensuring uniform dispersion of the sparks and heat generated. In addition to this, the machining and modified surface responses are altered when different concentrations of the conductive powders are applied [1, 3–5, 8, 9, 13, 14].

Non-dominated sorting genetic algorithm-II (NSGA-II) is known as rapid sorting and one of Dr. Deb's best multi-objective genetic algorithms that can simultaneously optimize the targets without being dominated by the other solution sets. NSGA-II possesses three particular features: (a) fast nondominated sorting method, (b) fast crowded distance assessing technique, and (c) simple crowder comparison operator. There are several multi-objective optimization methods including a multi-objective genetic algorithm (MOGA), micro-genetic algorithms (Micro-GA), strength Pareto evolutionary algorithm (SPEA), and Pareto archived evolution strategy (PAES) which are utilized in machining process variable optimization. NSGA-II as an updated form of MOGA is very popular and the most reliable multi-objective optimization method which can be employed in finding the best solution sets based on the optimal combinations of process variables. The literatures report that NSGA-II has been successfully utilized in advanced machining processes such as EDM and WEDM (wire-cut EDM) to optimize the responses showing the contradictory behavior between them [1, 15–17]. Kalyanmoy et al. [15] claimed that NSGA-II outperformed PAES and SPEA in terms of finding various data sets when several experimental problems were simulated. Although NSGA-II offers the best-fitted solution sets of the responses based on the set objective functions through the Pareto frontiers, it is very challenging to satisfy different objective functions concurrently. To overcome the challenges, several multi-criteria decision-making tools including the linear programming technique for multidimensional analysis of preference (LINMAP) and technique for order performance by similarity to ideal solutions (TOPSIS) are used to find out the best set of solution among the solution sets obtained from the Pareto frontiers. The LINMAP method is one of the most popular ideal seeking techniques for multi-criteria decision-making problems which has attained the attention of the researchers [18, 19].

The primary aim of this research is to enhance the machining and modified surface responses by increasing MRR and minimizing both SR and RLT while machining 316L steel through the multi-walled carbon nanotube (MWCNT)-suspended EDM process. Another goal of this study is to investigate the effects of MWCNT addition and the associated process variables of the EDM system on the machining and altered surface responses. The final goal includes predicting

optimal combinations of the process variables which offer the best-fitted solution sets for the responses. It is hypothesized that the addition of nano-sized MWCNT in the EDM oil improves the machining performances significantly because of attributing high electrical conductivity and thermal conductivity of 109 A/cm^2 and 3320 W/mk respectively. Furthermore, it can continuously float in the EDM oil which facilitates uniform dispersion of it through the machining gap because of having a low specific gravity and a high shape factor of more than one [20, 21]. It has been reported by Al-Amin et al. [4] that the machining gap may enlarge at most $125 \text{ }\mu\text{m}$ by applying the conductive particles in the EDM oil which results excellent machining stability, reduction in both RLT and SR, and increment of MRR by improving the flushing of the debris produced and ensuring multiple sparks formation through a single discharge. However, the overall system efficiency and the measures of machining responses highly depend on the EDM process variables which are categorized into two groups including electrical and non-electrical. Since the EDM technique works with stochastic behavior during the operation, optimization of the associated process variables is required to obtain the optimal machining responses. The electrical variables including peak current, duty cycle, and pulse-on time of the EDM process were preferred for this research because of their momentous influences on both machining and surface responses [1, 4, 5, 8, 9, 20, 21]. The approaches such as RSM, Taguchi, and Grey relational analysis are carried out only for the single-objective-based works [22, 23]. This research work has used a superior multi-objective optimization technique called NSGA-II to predict the optimal combinations of process variables for the best solution sets as there are conflicting behaviors between the machining responses. This research offers an advanced and cost-effective manufacturing method as well as suggests the optimal solution sets to the

process engineers for processing 316L steel with the desired machining and surface responses.

2 Experimental procedure

Overall, 316L steel was processed through the MWCNT-mixed EDM technique. In total, nine experiments were conducted in the present work. The machined 316L steel was prepared to measure SR, RLT, and surface morphology. Afterwards, the statistical analyses were carried out to investigate the influences of process variables on MRR, SR, and RLT. Multiple-objective optimization of the process factors was conducted through the NSGA-II technique to obtain the Pareto frontiers showing the optimal solution sets for the machining responses. Finally, a decision-making tool called the LINMAP method was utilized to find out the best solution set for the responses.

2.1 Materials and process

A CNC die-sinker EDM (model: FP60EA; brand: Mitsubishi; country of origin: Japan) was employed for machining 316L steel. EDM-oil (mineral oil) having a dielectric strength of 45 KVA has been used as the working dielectric. To ensure the consistent supply of MWCNT-mixed EDM oil to the working tank having a capacity of 200 l, a separate tank with a storage capacity of 20 l was adopted. Figure 1 shows a schematic model of the PM-EDM method. For all of the experiments, a cutting depth of 0.7 mm was carried out retaining a machining gap of 0.01 mm between the specimen and the tool electrode. A positive tool polarity with a constant gap voltage of 150 V was applied.

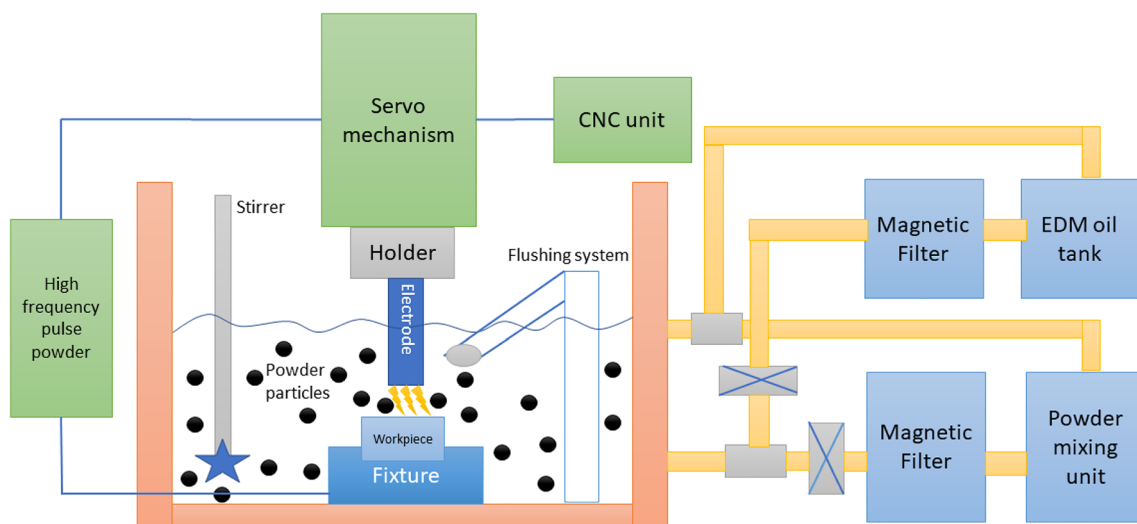
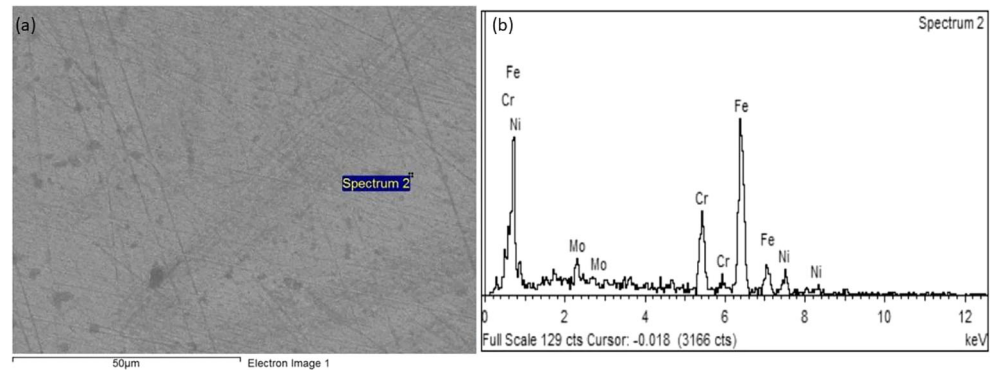


Fig. 1 A schematic model of the PM-EDM method [reproduced with permission from ref. [1]]

Fig. 2 As-received 316L steel a surface morphology using SEM; b elemental composition analysis using EDX spectrum



A surgical grade 316L steel (dimension: $5 \times 400 \times 400$ mm) bought from Mechatech solution, Malaysia, was employed as a specimen that was cut into the pieces (dimension: $5 \times 9 \times 10$ mm) using the wire-cut EDM method. Morphological and elemental analyses of the purchased 316L steel were carried out using the scanning electron microscopy (SEM) and the energy dispersive X-ray (EDX) analysis respectively as given in Fig. 2a-b. From Fig. 2a, a smooth surface of as-received 316L steel is noticed. The elemental composition analysis using the EDX confirms the existence of Fe, Cr, Ni, and Mo on the purchased 316L steel shown in Fig. 2b. Pure titanium was chosen as a tool electrode because of attributing low erosion rate and the hard carbides formation capability [1, 14]. The as-received pure titanium plate was sliced into the pieces of $85 \times 9.5 \times 10.5$ mm through the wire-cut EDM technique as well. The tool electrode faces formed were further polished using the polishing process to make them smooth. MWCNT with 91.35% purity bought from Mechatech solution, Malaysia, was selected as the additive. The purity of MWCNT was measured using thermogravimetric analysis (TGA) maintaining a temperature range: 25–900 °C and a temperature increment range: 10 °C/min. The TGA analysis reports 91.35% purity of the as-received MWCNT presented in Fig. 3.

2.2 Empirical design using the Taguchi approach

Because of cost and time constraints, the Taguchi-based design provides a robust design of experiments (DOE) with the least amount of possible experiments to obtain the best responses. This method offers an orthogonal array to construct the experimental design and signal-to-noise ratio (S/N) to achieve the optimal combinations of process variables for the desired responses [1, 24]. Taguchi-based L9 (3^4) approach was developed using Minitab 19 pro software which decreased the experimental cost and time by reducing the number of experiments. Levels of the selected variables are provided in Table 1. The mathematical modeling, analysis of variance (ANOVA), and influences of the variables on the machining and modified surface responses were carried out using Minitab 19 pro software. The process variables including peak current (A), pulse-on time (μ s), MWCNT amount (g/l), and duty cycle (%) were chosen to inspect their influences on the machining and modified surface responses such as MRR, RLT, and SR through extensive literature studies and adequate trial experimentations. The maximization was considered for MRR, whereas the minimization was preferred for both SR and RLT. Signal-to-noise ratio (S/N) is a quality loss

Fig. 3 TGA analysis of as-received MWCNT powder

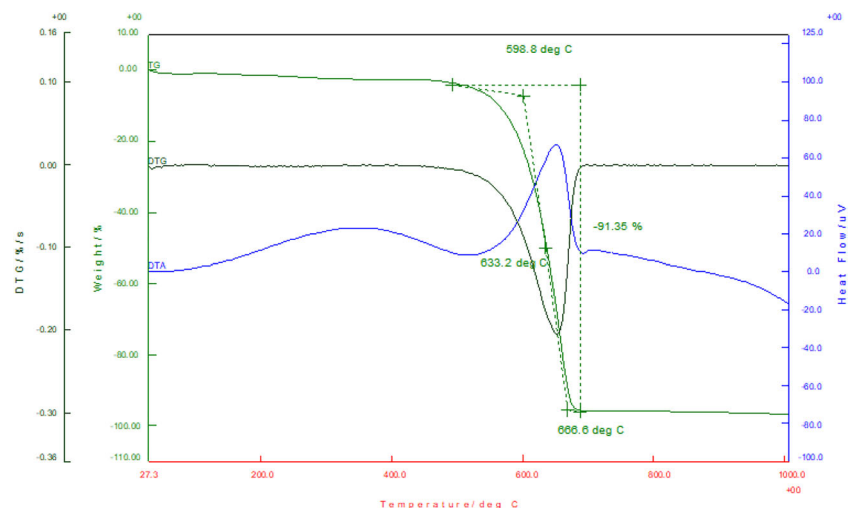


Table 1 Levels of the assigned manufacturing process factors

| Factors | Unit | Levels | Symbol |
|---------------|------|-------------|--------|
| Peak current | A | 5; 7; 10 | A |
| Pulse-on time | μs | 8; 12; 16 | B |
| MWCNT amount | g/l | 0.4; 0.7; 1 | C |
| Duty cycle | % | 40; 45; 55 | D |

function which was calculated using the given mathematical equations (Eqs. (1) and (2)).

The largest-the-better

$$S/N = -10\log \left[\frac{1}{n \sum_{i=1}^n y^2} \right] \tag{1}$$

The smallest-the-better

$$S/N = -10\log \left[\frac{1}{n \sum_{i=1}^n y^2} \right] \tag{2}$$

where *y* represents the *n*th observations of MRR, SR, and RLT.

The non-linear with first order mathematical models were developed following Eq. (3)

$$Y = \beta_0 + \sum_{i=1}^n \beta_i X_i + \sum_{i < j=2}^n \sum_{j=2}^n \beta_{ij} X_i X_j + \alpha \tag{3}$$

where *Y* is the response, β is the regression coefficient, *n* is the number of independent factor, *X* denotes independent factors, and α provides an error value.

Duty cycle is measured using Eq. (4)

$$\text{Duty cycle} = (\text{pulse-on time} / \text{total cycle time}) \times 100\% \tag{4}$$

where total cycle time represents the summation of pulse-on time and pulse-off time.

2.3 Measurement of the machining and modified surface responses

2.3.1 Material removal rate

MRR was measured using Eq. (5)

$$\text{MRR} = (M_b - M_a) / \text{machining time} \tag{5}$$

where *M_b* = mass of the workpiece before machining and *M_a* = mass of the workpiece after machining. Machining time refers a certain duration for completing a job or machining. A high-accuracy digital mass measuring machine (Model: Mettler Toledo ME3002) having a resolution of 0.01 g was employed to calculate *M_b* and *M_a*.

2.3.2 Surface roughness

A profilometer (Brand: Mitutoyo; Model: SV3000; Origin: Japan) with a resolution of 0.05 μm was utilized to estimate the arithmetic roughness (Ra). The measurement of SR was carried out obeying ISO 3274-1996 standard. The stylus travel length of 7 mm was considered to conduct the tests. When the stylus reaches the travel length considered, the vertical movement of it is converted into electrical signal through the in-built transducer and displayed as the roughness profile.

2.3.3 Recast layer thickness

The machined 316L steel samples were mounted on the mounting press machine (Model: Simplimet@1000; Origin: USA). The mounted specimens were polished employing the SiC grinding papers including 400, 600, 800, 1200, and 1500 grits periodically through the grinder-polisher machine (Model: Metaserv250). The specimens polished were chemically treated by the Carpenters etchant solution (FeCl₃: 8.5 gm; ethanol: 122 ml; hydrochloric acid: 122 ml; CuCl₂: 2.4 gm; Nitric acid: 6 ml) for 3 s to avoid the debris and the burrs. The polished and etched specimens were explored to estimate the recast layer thickness through the SEM technique (Brand: Phenom; Model: Pro X; Origin: Netherlands) applying extra high tension (EHT) powder supply ranging from 5 to 15 KV and magnification varying from × 500 to × 1500. Surface morphology was carried out by the SEM technique (Model: Zeiss Evo LS15; Origin: Germany) as well applying EHT powder supply of 5 KV to investigate the microcracks, pores, and craters on the modified 316L steel surface. The EDX spectrum method was used to identify the elemental composition of the treated surface.

2.4 Multi-objective optimization using established NSGA-II

The multi-objective such as maximizing MRR and minimizing both SR and RLT optimization of the process variables was performed through the NSGA-II technique which is widely used as the multi-objective optimization tool. This technique enables optimization of the set objective functions without being dominated by the other solution sets. Pareto optimal frontiers displaying the obtained optimal solution sets were generated using the MATLAB software. Figure 4 shows the flowchart of the NSGA-II technique. Table 2 presents the required variables setting to perform the NSGA-II technique. To choose the best solution set of the responses based on the set objective functions, the most widely used decision-making technique called LINMAP was applied in this research. The solution set that was located at the least distance from the imaginary reference point (called ideal point) sketched from the extreme points A and B was considered as the best-fitted

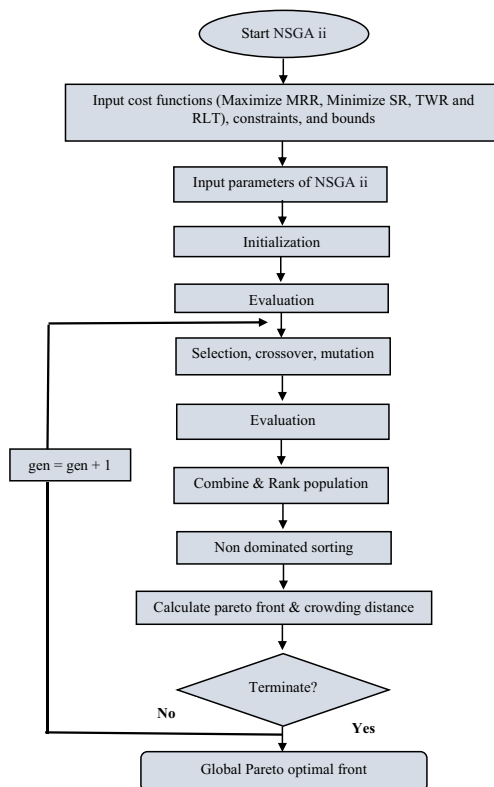


Fig. 4 Flowchart of the NSGA-II technique

solution set [1]. Based on the LINMAP technique, the distance between the sketched reference point and any solution set in the Pareto frontier can be measured using Eq. (6) [25].

$$E_{di+} = \sum_{j=1}^m \left(F_{ij} - F_j^{\text{ideal}} \right)^2, \quad i = 1; \dots; n \quad (6)$$

Here, m presents objectives number, i indicates each solution of the Pareto front, and F_j^{ideal} refers to the ideal value.

Table 2 Variable setting for NSGA-II application

| Selected parameters | Measurement |
|-----------------------|----------------------|
| Population mode | Double vector |
| Population size | 300 |
| Selection | Tournament |
| Crossover percentages | 0.9 |
| Crossover mode | Intermediate |
| Crossover ratio | 1 |
| Mutation | Constraint dependent |
| Pareto fraction | 0.6 |
| Migration | Forward |
| Migration fraction | 0.1 |

3 Results and discussion

This part describes the experimental data achieved by conducting the nine experiments using the Taguchi-based L9 (3^4) model. In addition to this, it is structured to reveal the key findings that support the research questions, purpose statement, and methodology of this work. Table 3 demonstrates the L9 design with experimental results and the S/N ratio for the machining responses.

3.1 Signal-to-noise analysis for the performances

The function of quality loss is referred to as the S/N ratio that is a continuous function that refers to the deviations of a designed factor from its absolute value. Larger S/N values provide the desired combination of the process variables for the optimal machining responses [24]. As larger MRR and lower both RLT and SR were the preferred modes of the machining responses, the greater-the-better and the lower-the-better were considered for MRR, and SR and RLT respectively. From Table 3, run_9 displays the highest S/N ratio for MRR. Therefore, a 10-A peak current, 16- μ s pulse-on time, 1-g/l MWCNT amount, and 45% duty cycle provided the optimal combination of the factors for maximizing MRR. On the other hand, run_1 shows the highest S/N ratio for both SR and RLT. Hence, the optimal combination of process variables for minimizing both RLT and SR was achieved corresponding to a peak current of 5 A, MWCNT amount of 0.7 g/l, pulse-on time of 8 μ s, and duty cycle of 45%.

3.2 Main effects analysis and mathematical model development for the performances

The main effects plots of the responses shown in Fig. 5a–c demonstrate peak current, MWCNT amount, and pulse-on time being influential for all the responses. However, the duty cycle shows an influential factor only for SR. In addition to this, the MWCNT amount displays a reverse trend for RLT with respect to the peak current and pulse-on time. The most influential variable for all the responses indicates toward the peak current followed by the MWCNT amount, pulse-on time, and duty cycle. From Fig. 5a, the largest MRR is achieved corresponding to a peak current of 10 A, pulse-on time of 16 μ s, MWCNT amount of 1 g/l, and duty cycle of 40%. The smallest SR is obtained at a 5-A peak current, 8- μ s pulse-on time, 0.4-g/l MWCNT amount, and 40% duty cycle as shown in Fig. 5b, but the minimum RLT is measured when the MWCNT amount and duty cycle improve to 1 g/l and 45% respectively as depicted in Fig. 5c.

The normal probability plots depicted in Fig. 6a–c show that the residuals lie on the reference lines which

Table 3 L9 design with experimental results and S/N ratio for all the responses

| Run | Process factors | | | | Responses | | | | | |
|-----|-----------------|--------|---------|------|--------------|-------------------|--------------|------------|-----------------|-------------------|
| | A (A) | B (μs) | C (g/l) | D | MRR (mg/min) | S/N ratio for MRR | SR (Ra) (μm) | S/N for SR | RLT (avg.) (μm) | S/N ratio for RLT |
| 1 | 5 | 8 | 0.7 | 0.45 | 4.20 | 12.46 | 1.58 | - 3.97 | 5.243 | - 14.39 |
| 2 | 5 | 12 | 1 | 0.40 | 6.86 | 16.73 | 1.78 | - 5.09 | 6.24 | - 15.90 |
| 3 | 5 | 16 | 0.4 | 0.55 | 4.85 | 13.71 | 1.88 | - 5.51 | 9.25 | - 19.32 |
| 4 | 7 | 8 | 1 | 0.55 | 12.10 | 21.65 | 2.27 | - 7.12 | 7.37 | - 17.34 |
| 5 | 7 | 12 | 0.4 | 0.45 | 8.25 | 18.33 | 2.02 | - 6.11 | 12.37 | - 21.84 |
| 6 | 7 | 16 | 0.7 | 0.40 | 17.88 | 25.05 | 2.15 | - 6.65 | 11.87 | - 21.49 |
| 7 | 10 | 8 | 0.4 | 0.40 | 19.23 | 25.68 | 2.23 | - 6.97 | 15.56 | - 23.84 |
| 8 | 10 | 12 | 0.7 | 0.55 | 30.25 | 29.61 | 2.77 | - 8.90 | 14.35 | - 23.14 |
| 9 | 10 | 16 | 1 | 0.45 | 42.25 | 32.52 | 2.85 | - 9.10 | 14.15 | - 23.02 |

indicate the model terms selected being the only important variables and the errors are normally distributed [26].

Finally, the general form of non-linear mathematical models for MRR, SR, and RLT was developed to carry out the multi-objective optimization through NSGA-II which are given as follows:

$$MRR = 3.9 + 1.57*A - 2.83*B - 53.5*C + 35.1*D + 0.095*A*B + 1.81*A*C + 4.55*B*C$$

$$SR = -0.863 + 0.153*A + 0.0597*B + 1.604*C + 1.081*D$$

$$+ 0.00522*A*B - 0.032*A*C - 0.0875*B*C$$

$$RLT = -5.78 + 1.952*A + 0.843*B + 7.7*C - 10.7*D + 0.0095*A*B - 0.46*A*C - 0.82*B*C$$

where *A* = peak current (A), *B* = pulse-on time (μs), *C* = MWCNT amount (g/l), and *D* = duty cycle.

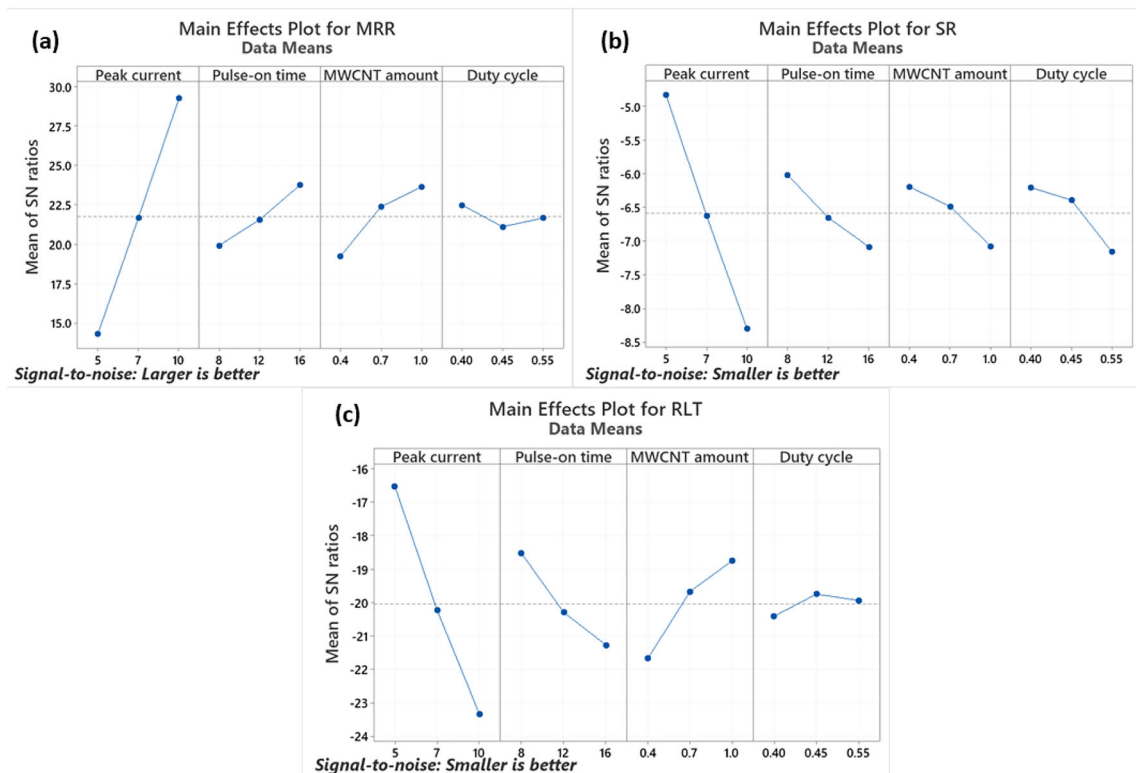


Fig. 5 Main effects plots of **a** MRR, **b** SR, and **c** RLT

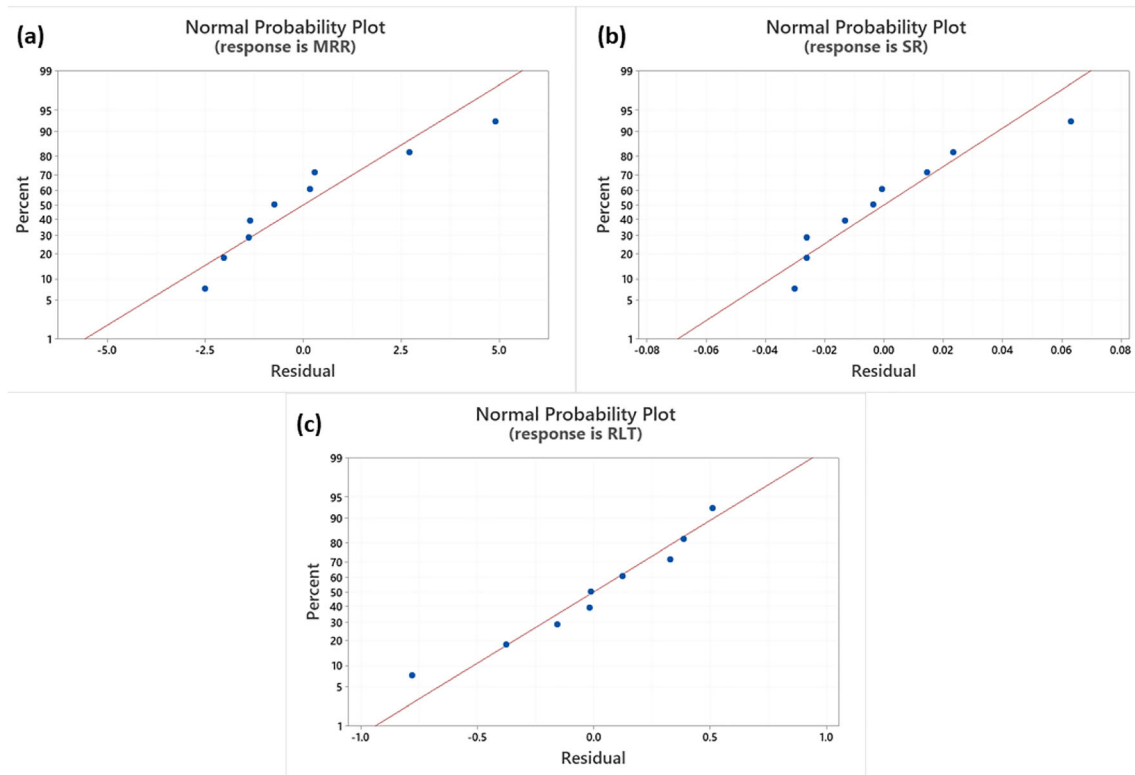


Fig. 6 Normal probability plots of **a** MRR, **b** SR, and **c** RLT

3.3 Investigation of MRR results

3.3.1 ANOVA analysis

A summary of the ANOVA analyses for all the responses is shown in Table 4. The confidence level of 95% or 5% significance ($\alpha = 0.05$) was considered to analyze the models [5]. From Table 4, the values of R -sq (Adj) and R -sq are 93.04% and 96.62% respectively which ensure the regression model providing excellent analysis of the process factors for MRR. Since the p values of the peak current (0.001), MWCNT amount (0.024), and pulse-on time (0.026) are smaller than 0.05, these process factors are statistically significant for MRR which acknowledge the previous studies [1, 5, 9, 26, 27]. The factors such as A , B , and C contribute by 75.15%, 10.47%, and 10.88% respectively to MRR. Hence, the suspended MWCNT along with discharge energy influences MRR.

3.3.2 Impacts of manufacturing process variables on MRR

A contour plot provides a 2D presentation of two variables for a response where the response with the different ranges is combined to produce a constant contour line [22]. The contour plots shown in Fig. 7a–c represent the combined impacts of the related variables on MRR. From Fig. 7a, the highest MRR of more than 40 mg/min is observed at a pulse-on time and peak current ranging from 15.2 to 16 μ s and from 9.7 to 10 A respectively, whereas the smallest value of MRR (less than 10 mg/min) is observed at a peak current ranging from 5 to 7.5 A and all the pulse-on time values (from 8 to 16 μ s). MRR improves from 20 to 30 mg/min while pulse-on time raises from 8.3 to 16 μ s with the increment of peak current from 7.5 to 10 A. As shown in Fig. 7b, the lowest MRR of less than 10 mg/min is obtained at a peak current ranging from 5 to 7.5 A with all MWCNT amount values (0.4 to 1 g/l). However, the

Table 4 Summary of the ANOVA analysis for all the performances

| Responses | Factors with p value | | | | Model accuracy | | Contribution | | | |
|----------------|------------------------|-------|--------|-------|----------------|----------------|--------------|--------|--------|-------|
| | A | B | C | D | R -sq (%) | R -sq (adj%) | A | B | C | D |
| MRR (mg/min) | 0.001 | 0.026 | 0.024 | 0.894 | 96.52 | 93.04 | 75.15% | 10.47% | 10.88% | 0.02% |
| SR (μ m) | 0.0001 | 0.001 | 0.0015 | 0.002 | 99.5 | 99 | 78.32% | 7.53% | 6.90% | 6.75% |
| RLT (μ m) | 0.0001 | 0.007 | 0.003 | 0.145 | 98.87 | 97.47 | 77.84% | 7.25% | 12.76% | 0.92% |

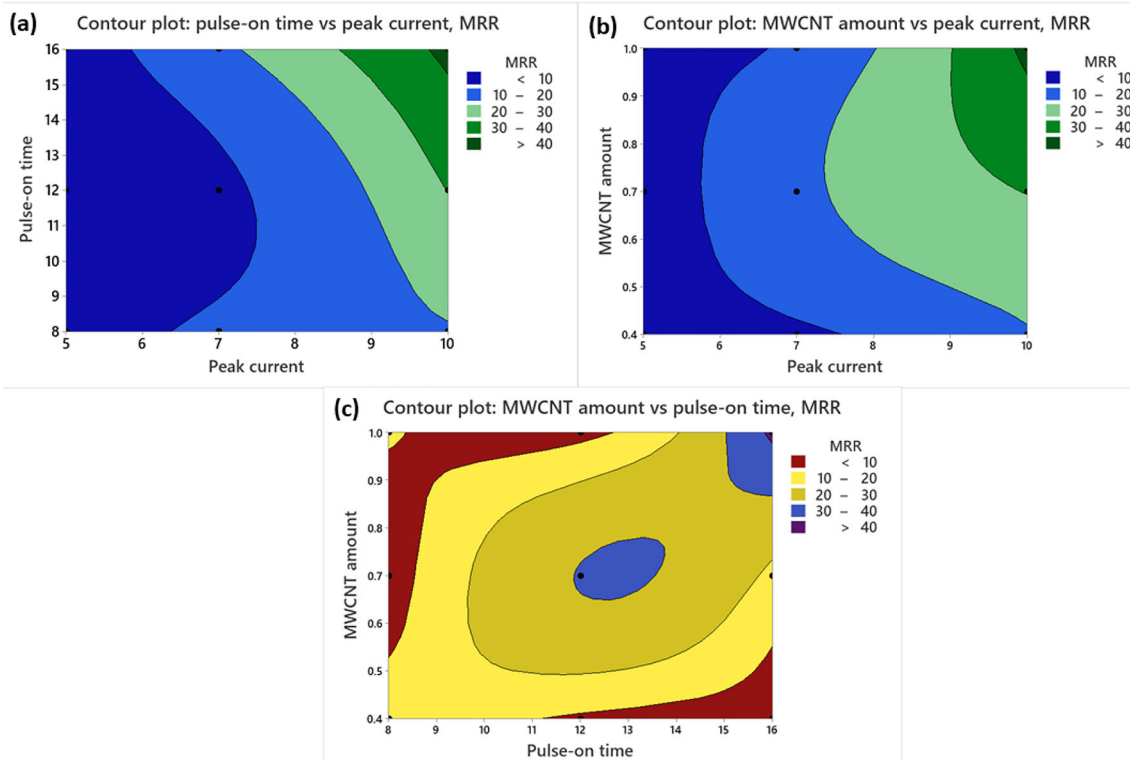


Fig. 7 The combined effects of process variables on MRR **a** B vs A, **b** C vs A, and **c** C vs B

largest MRR of more than 40 mg/min is found corresponding to a peak current of almost 10 A and MWCNT amount of more than 0.90 g/l. MRR ameliorates from 30 to 40 mg/min when the peak current and MWCNT amounts increase from 9.1 to 10 A and from 0.7 to 1 g/l respectively. In Fig. 7c, an MRR of more than 40 mg/min is noticed at a pulse-on time of 16 μ s and an MWCNT amount of 1 g/l while an MRR of less than 10 mg/min is observed at all the values of both the MWCNT amount and pulse-on time. MRR increases from 30 to 40 mg/min not only at a pulse-on time ranging from 12 to 14 μ s and the MWCNT amount varied from 0.65 to 0.75 g/l but also the corresponding to an MWCNT amount which varied from 0.85 to 1 g/l and pulse-on time ranged from 14.8 to 16 μ s.

The 3D surface plots for MRR are demonstrated in Fig. 8a–c by changing two factors while the other factors remained constant [26]. As shown in Fig. 8a, overall, an upward trend of MRR is displayed with the improvement of both pulse-on time and peak current. A sudden decline in MRR is observed at a peak current of 7 A and a pulse-on time of 12 μ s. The largest MRR is measured at a 10-A peak current and 16- μ s pulse-on time, whereas the smallest MRR is calculated at a 5-A peak current and 8- μ s pulse-on time. From Fig. 8b, it is clearly seen that MRR ameliorates by the augment of both MWCNT amount and peak current. A higher MRR is calculated corresponding to a 0.7-g/l MWCNT amount compared to the 1-g/l MWCNT amount with the applied peak current of

7 A. MRR increases at MWCNT amount of 1 g/l with all peak current values except peak current of 7 A, whereas it decreases at an MWCNT amount of 0.4 g/l with all peak current values. The intersecting points of (5-A peak current, 0.4-g/l MWCNT amount) and (10-A peak current, 1-g/l MWCNT amount) reveal the lowest and highest MRR respectively. In Fig. 8c, overall, an upward trend of MRR is observed when the pulse-on time rises with the increment of the MWCNT amount. A higher MRR is estimated at a pulse-on time of 8 μ s and MWCNT amount of 1 g/l than MRR obtained at a pulse-on time of 12 μ s and MWCNT amount of 0.4 g/l. The smallest MRR is found corresponding to a pulse-on time of 8 μ s and an MWCNT amount of 0.7 g/l while the largest MRR is noticed at a pulse-on time of 16 μ s and an MWCNT amount of 1 g/l.

From the aforesaid analysis in this section, it can be concluded that MRR ameliorates when both peak current and pulse-on time rise due to increasing the conversion of the electrical sparks applied into the heat energy in the plasma channel. A high duty cycle application with high both peak current and pulse-on time may occur in unstable machining which may reduce material removal because of poor flushing resulting in a short circuit caused by the unremoved debris in the machining gap. Introducing the MWCNT particles in the working fluid with low discharge energy application ameliorates MRR due to the bridging effects between the energized particles resulted from the capacitive effects. In addition to

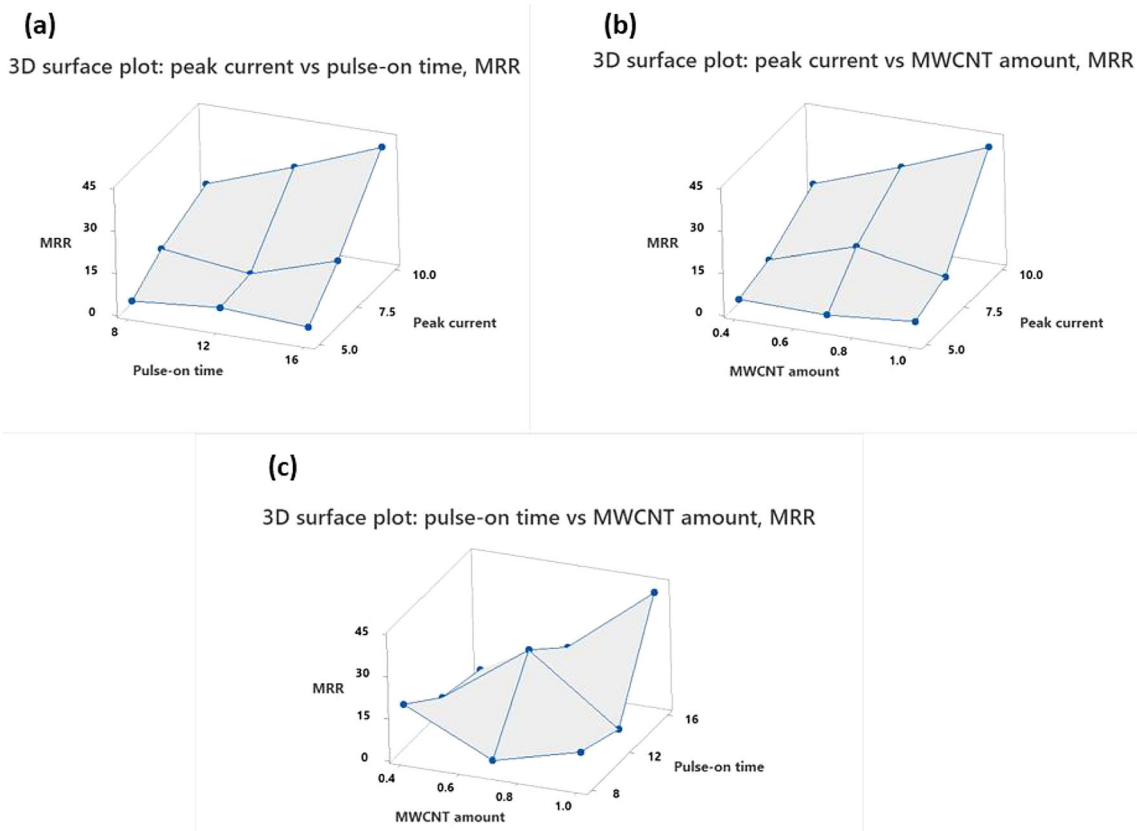


Fig. 8 3D surface plots for MRR **a** A vs B, **b** A vs C, and **c** B vs C

this, the bridging effects generate multiple ignitions in the machining gap by the single discharges which cause more material removal. The addition of highly electrical-conductive MWCNT additive enlarges the machining gap facilitating a stable and smooth operation because of improving the flushing performance. When MRR increases, the produced debris leads to rubbing phenomena due to the magnetic and turbulence effects in the machining gap which improves MRR further [4, 8, 9, 13, 26–29]. However, a few research works have shown a reduction in MRR applying thermally and electrically conductive additives in the working liquid due to the dispersion of electrical sparks and thermal energy generated during the operation [30–32]. The present research has obtained comparatively higher MRR with less discharge energy application than the previous studies [5, 9, 26–29, 33].

3.4 Investigation of SR results

3.4.1 ANOVA analysis

From Table 4, the values of R -sq (Adj) and R -sq are 99.00% and 99.5% respectively that guarantee the regression model offering strong analysis of the process variables for SR. As p values of peak current (0.0001), MWCNT amount (0.0015), pulse-on time (0.001), and duty cycle (0.002) are lower than

0.05, these parameters are statistically momentous for SR. The related process factors such as A, B, C, and D contribute by 78.32%, 7.53%, 6.90%, and 6.75% respectively to SR. It is explicit that the added MWCNT particles with discharge energy affect SR.

3.4.2 Impacts of manufacturing process variables on SR

The combined impacts of the associated variables on SR are reflected by the contour plots depicted in Fig. 9a–c. As shown in Fig. 9a, the smallest SR is noticed at a 5-A peak current and the pulse-on time of 8 μ s while SR shows the highest values corresponding to a peak current of around 10 A and pulse-on time of more than 12 μ s. SR increases from 1.6 to 2.6 μ m when peak current augments from 5.5 to 10 A with all the inputs of pulse-on time. From Fig. 9b, at the lowest peak current of 5 A with MWCNT amount ranged from 0.65 to 0.8 g/l, SR shows the lowest values that are remarked by the dark blue color. Further increment of the peak current to 10 A with all MWCNT amounts (from 0.4 to 1 g/l) results in a rise of SR ranging from 1.6 to 2.8 μ m. The dark green region displays the highest SR obtained due to high both peak current and MWCNT amount applications. In Fig. 9c, the smallest SR is observed for the lowest pulse-on time values and MWCNT amount of 0.7 g/l that is indicated by the dark red color zone.

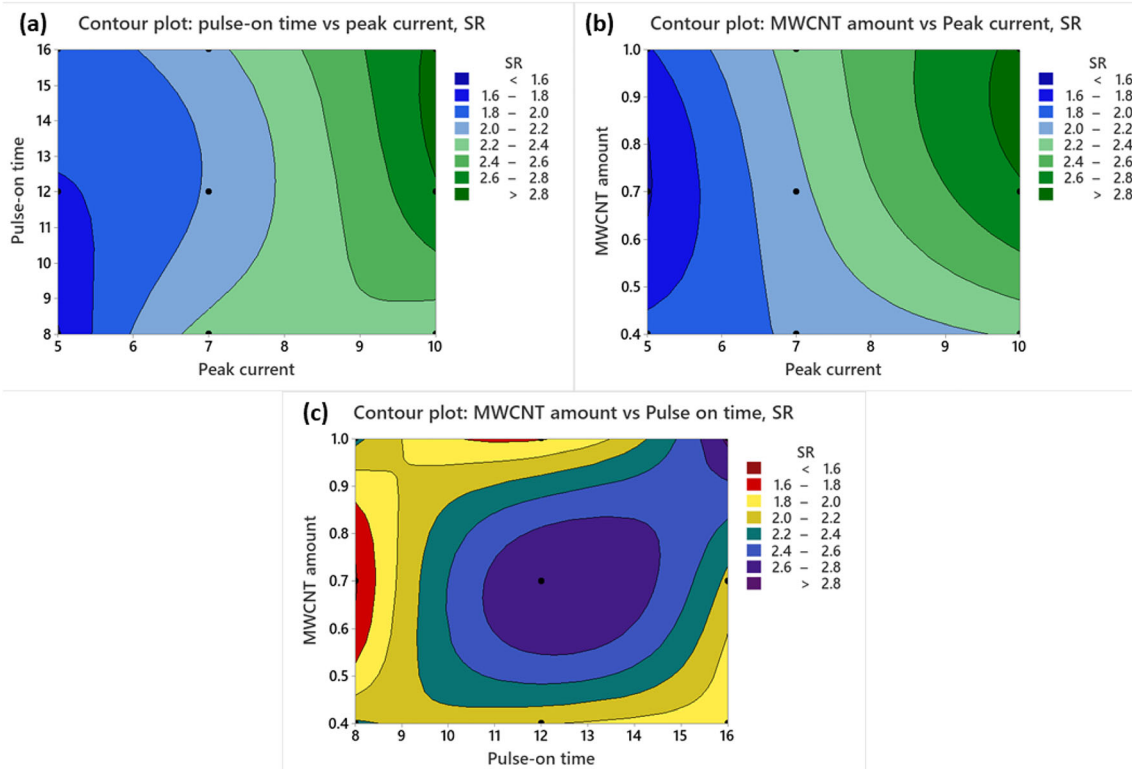


Fig. 9 The combined effects of process variables on SR **a** B vs A, **b** C vs A, and **c** C vs B

Further increment of pulse-on time to 16 μ s with all MWCNT amount inputs measures a rise in SR ranging from 1.6 to 2.8 μ m. SR reveals the maximum where the combination of pulse-on time and MWCNT amount is the maximum that is marked by the purple color.

From the 3D plot in Fig. 10a, it is outright said that SR improves due to the increment of both peak current and pulse-on time. The biggest SR is measured for a 10-A peak current and pulse-on time of 16 μ s, whereas the lowest SR is obtained at a peak current of 5 A and pulse-on time of 8 μ s. A higher SR is observed at a 7-A peak current and pulse-on time of 8 μ s compared to the obtained SR corresponding to a peak current of 7 A and pulse-on time of 12 μ s. As shown in Fig. 10b, SR reveals an upward trend when the peak current and MWCNT amounts increase. The highest SR is measured at an MWCNT amount of 1 g/l and a peak current of 10 A although the smallest SR is found at an MWCNT amount of 0.4 g/l and a peak current of 5 A. A larger SR is calculated corresponding to a 7-A peak current and 1-g/l MWCNT amount compared to the obtained SR at a peak current of 7 A and an MWCNT amount of 0.4 g/l. In addition to this, a smaller SR is observed at a peak current of 5 A and MWCNT amount of 1 g/l than the measured SR at a 5-A peak current and 0.4-g/l MWCNT amount. From the 3D plot in Fig. 10c, SR improves with raising both pulse-on time and MWCNT amounts. SR reveals the greatest for a pulse-on time of 16 μ s and an MWCNT amount of 1 g/l, whereas it becomes the smallest

corresponding pulse-on time of 8 μ s and MWCNT amount of 0.7 g/l. A greater SR is obtained at a 8- μ s pulse-on time with a 1-g/l MWCNT amount compared to the obtained SR at a pulse-on time of 12 μ s with an MWCNT amount of 0.4 g/l while a smaller SR is observed at a pulse-on time of 12 μ s with an MWCNT amount of 1 g/l than the estimated SR corresponding to a 16- μ s peak pulse-on time and a 0.4-g/l MWCNT amount.

From the aforesaid analysis of this section, it is explicit that SR of the part machined increases with improving the discharge energy because of supplying more and large-sized electrical sparks in the machining gap resulting in deep craters and pores formation on the machined surface. In addition to this, unstable machining due to poor flushing of the debris produced may occur during the operation if the duty cycle is set high enough causing irregular sparks and deep craters formation. However, it is noticed that the increment of MWCNT amount with low discharge energy application reduces the SR because of declining the resistive strength of the EDM-oil and enlarging the discharge gap enough resulting in excellent flushing. Furthermore, the added MWCNT particles in the EDM-oil facilitate the creation of the narrow-sized multiple ignitions due to the formation of the bridging effects resulting in low SR by the single discharge. Though the increment of electrical energy creates large size electrical sparks, the addition of MWCNT powders abates SR following four fundamentals: (a) uniform dispersion of heat energy, (b) multiple

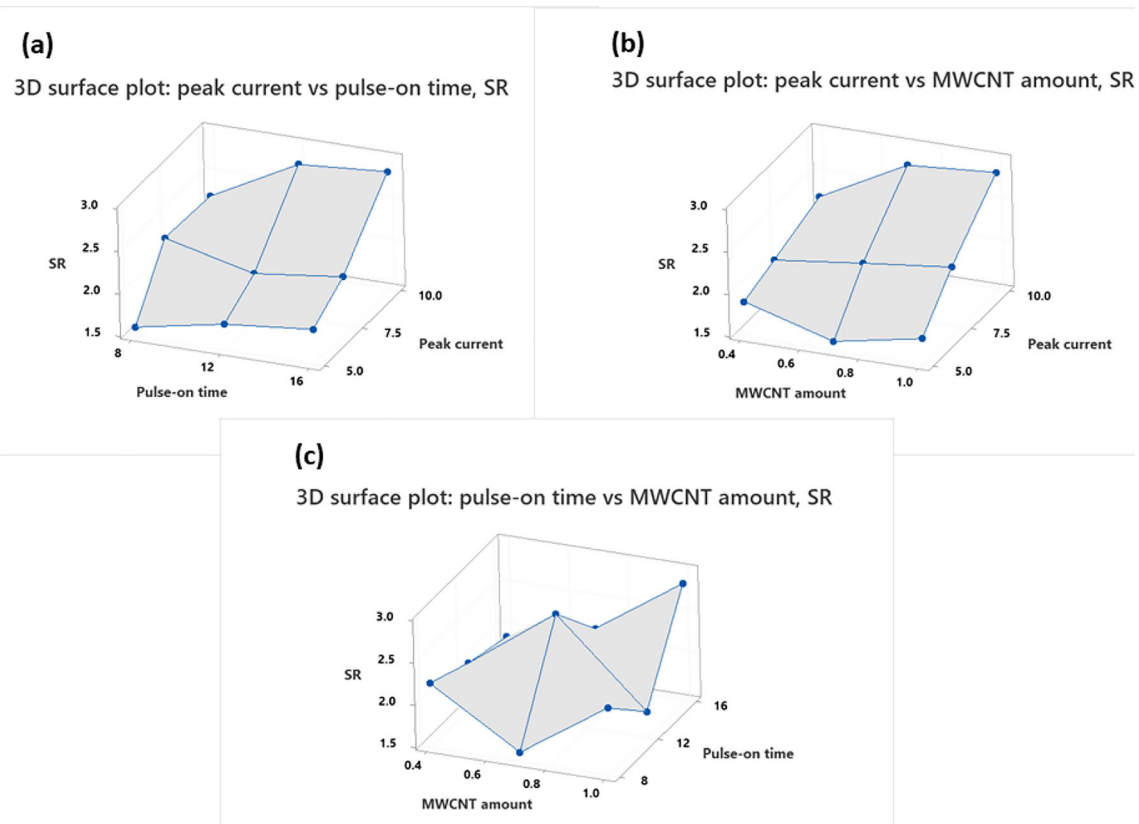


Fig. 10 3D surface plots for SR a A vs B, b A vs C, and c B vs C

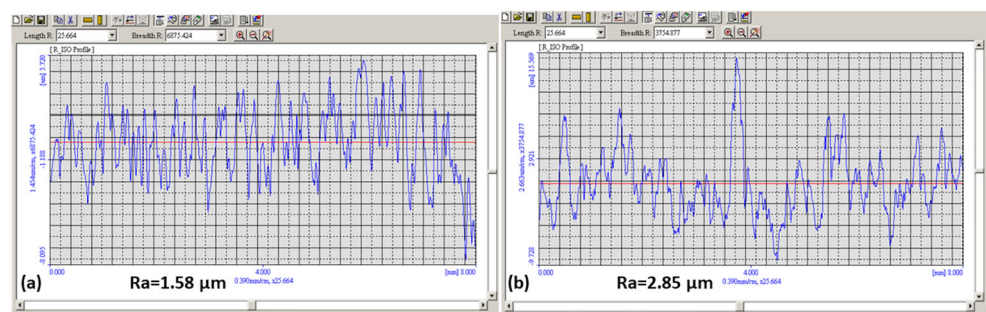
sparks formation from a long distance, (c) production of normal and uniform narrow sized sparks, and (d) scouring phenomena occurred by the produced debris due to magnetic and whirling impacts [4, 5, 9, 13, 20, 28, 29, 34]. This study showed comparatively lower SR than the previous investigations [5, 8, 21, 28, 29]. Figure 11a and b demonstrate the roughness profiles of the machined 316L steel at different parameter settings through the profilometer. In Fig. 11a, the largest SR of 2.85 μm is obtained at a peak current of 10 A, pulse-on time of 16 μs , MWCNT amount of 1 g/l, and duty cycle of 45%, whereas the smallest SR of 1.58 μm is measured corresponding to a 5-A peak current, 8- μs pulse-on time, 0.7-g/l MWCNT amount, and 45% duty cycle.

3.5 Investigation of RLT results

3.5.1 ANOVA analysis

From Table 4, the regression model offers a robust analysis of the related factors for RLT because the results of R -sq (Adj) and R -sq are 97.47% and 98.87% respectively. The variables such as peak current (0.0001), MWCNT amount (0.003), and pulse-on time (0.007) are statistically significant for RLT because the p values obtained of them being smaller than 0.05. Peak current, pulse-on time, and MWCNT amount contribute by 77.84%, 7.25%, and 12.76% respectively to RLT. It is clear that the added MWCNT shows a vital role in changing the RLT.

Fig. 11 Roughness profiles of the machined 316L steel at (a) peak current of 10 A, pulse-on time of 16 μs , MWCNT amount of 1 g/l, and duty cycle of 45% and (b) 5-A peak current, 8 μs pulse-on time, 0.7 g/l MWCNT amount, and 45% duty cycle



3.5.2 Impacts of manufacturing process variables on RLT

The combined impacts of the process factors on RLT are displayed in Fig. 12a–c. From the contour plot shown in Fig. 12a, the smallest RLT is noticed at a peak current ranging from 5 to 6 A and the pulse-on time varied from 8 to 11.2 μ s, whereas RLT becomes the highest when both peak current and pulse-on time augment from 8 to 10 A and from 8 to 16 μ s respectively. RLT increases from 6 to 12 μ m while improving both peak current from 5 to 8.8 A and pulse-on time from 8 to 16 μ s. In Fig. 12b, at the smallest peak current values and MWCNT amount ranging from 0.62 to 0.98 g/l, RLT shows less than 6 μ m that is marked by the dark blue color. Further augmentation of the peak current to 9.2 A with all MWCNT amount values (from 0.4 to 1 g/l) results in an increase of RLT ranging from 6 to 12 μ m. The dark green region reveals the maximum fitted values of the RLT corresponding to a peak current ranging from 8 to 10 A and the MWCNT amount varied from 0.4 to 1 g/l. As shown in Fig. 12c, RLT shows the lowest for pulse-on time ranged from 8 to 12 μ s and MWCNT amount ranged from 0.65 to 0.95 g/l which is highlighted by the dark red color. Further increment of pulse-on time to 16 μ s with all MWCNT amount inputs causes a rise of RLT varied from 6 to 14 μ m. The areas indicating an RLT of more than 14 μ m are marked in purple color.

The 3D surface plots for RLT are depicted in Fig. 13a–c. As shown in Fig. 13a, an upward trend of RLT is observed for

increasing both peak current and pulse-on time. RLT displays the greatest at the 8- μ s pulse-on time and the 10-A peak current, but it becomes the smallest corresponding to a peak current of 5 A and a pulse-on time of 8 μ s. A greater RLT is estimated at an 8- μ s pulse-on time with a 10-A peak current than the obtained RLT at a pulse-on time of 16 μ s and a peak current of 10 A. However, a lower RLT is calculated at a pulse-on time of 8 μ s with a peak current of 7 A than the measured RLT at a 16- μ s peak pulse-on time and a 7-A peak current. From the 3D plot in Fig. 13b, RLT improves when peak current increases and MWCNT amount decreases. The largest RLT is estimated at a peak current of 10 A and MWCNT amount of 0.4 g/l while it becomes the lowest at the peak current of 5 A and MWCNT amount of 0.7 g/l. A larger RLT is calculated at the 5-A peak current with the 0.4-g/l MWCNT amount compared to the obtained RLT corresponding to an MWCNT amount of 1 g/l and peak current of 7 A. As shown in Fig. 13c, RLT shows an upward trend when pulse-on time rises and MWCNT amount declines. The largest RLT is obtained at the pulse-on time of 8 μ s and MWCNT amount of 0.4 g/l while the lowest RLT is found at the pulse-on time of 8 μ s and MWCNT amount of 0.7 g/l. RLT becomes lower corresponding to a combination of an 8- μ s pulse-on time and 1-g/l MWCNT amount compared to the combination of 12 μ s and 0.4-g/l MWCNT amount.

It is summarized from this section that RLT improves when pulse-on time and peak current increase owing to increasing

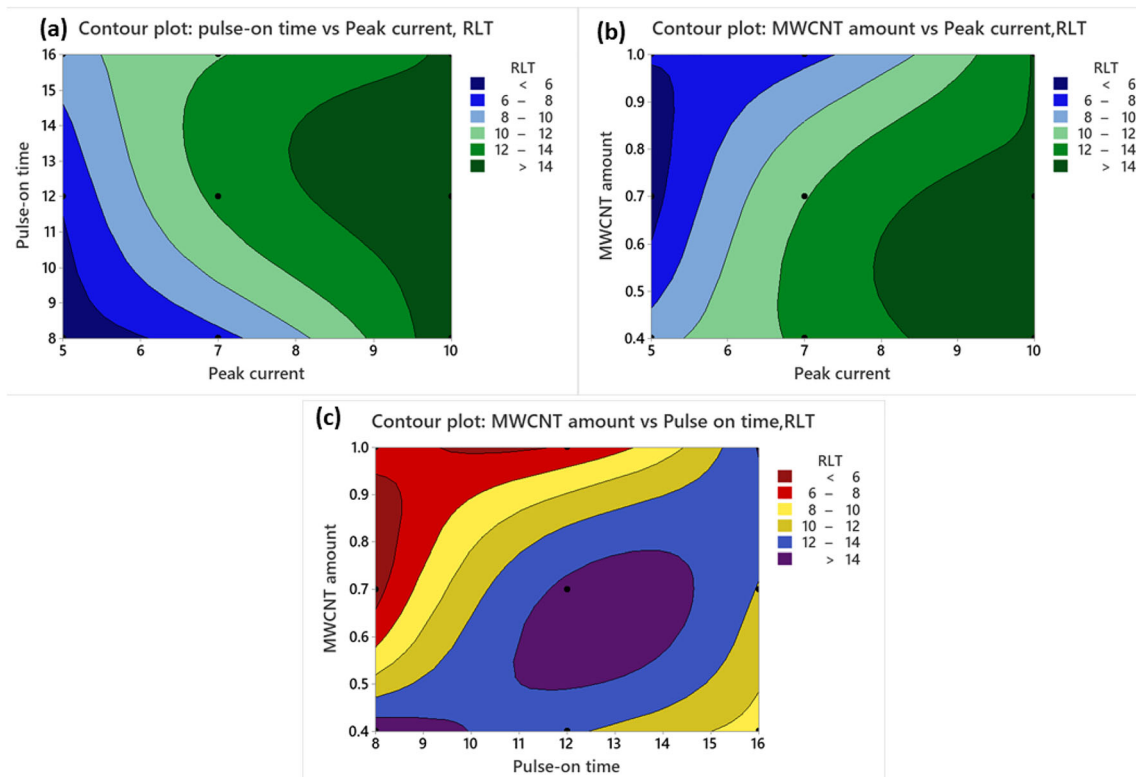
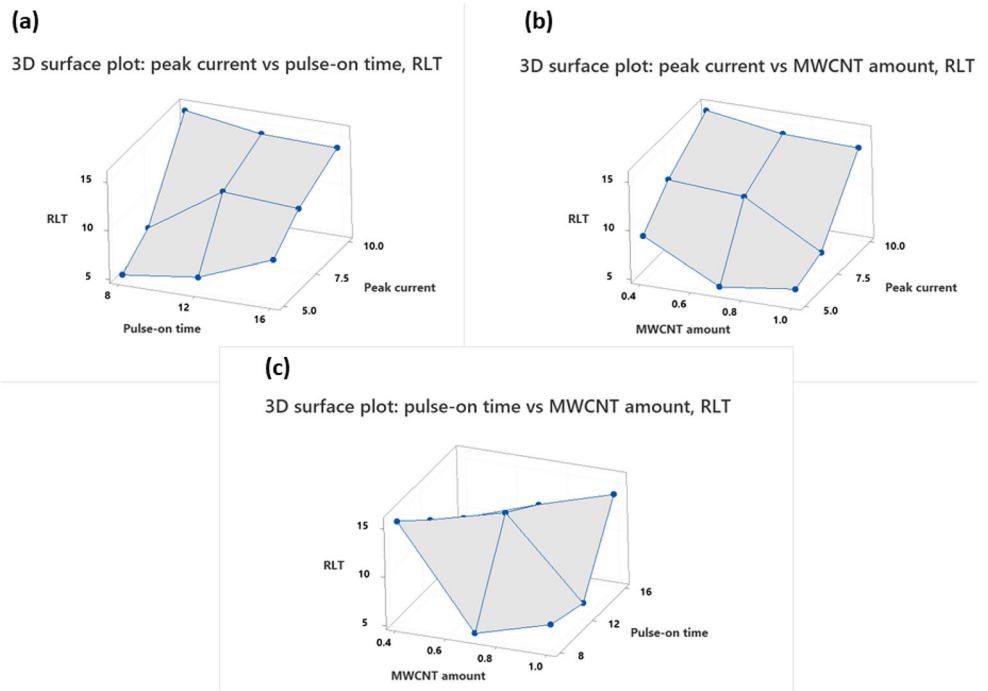


Fig. 12 The combined effects of process variables on RLT a B vs A, b C vs A, and c C vs B

Fig. 13 3D surface plots for RLT **a** A vs B, **b** A vs C, and **c** B vs C



the production and deposition of the debris eroded during the operation. Since more MRR occurs because of high electrical energy application rather than flushing of the produced debris, RLT ameliorates through rapid deposition and solidification of them during the machining. The migration of elements on the fabricated part during the operation is shown in Fig. 14.

From Fig. 14, it can be clearly identified the existence of C, Fe, Ti, Si, Cr, and Ni on the machined 316L steel which are migrated from the specimen, tool electrode, added MWCNT, and EDM-oil. It is noticed that the increment of MWCNT particles reduces RLT on the machined part because of the following fundamentals: (a) enlarging the machining gap

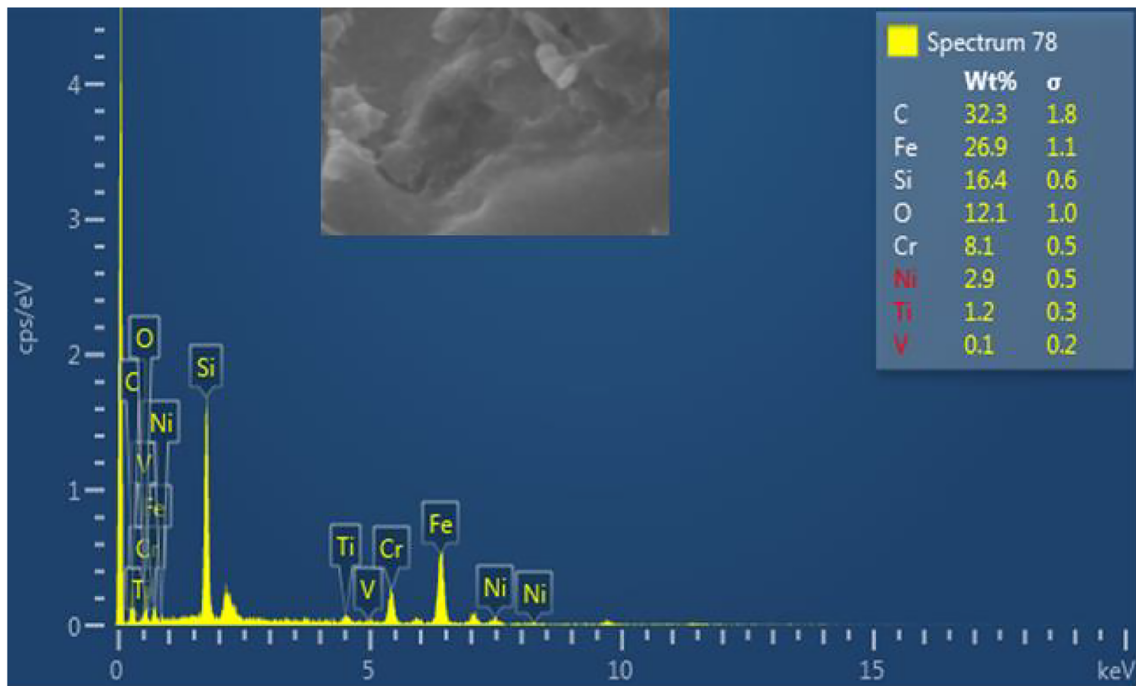
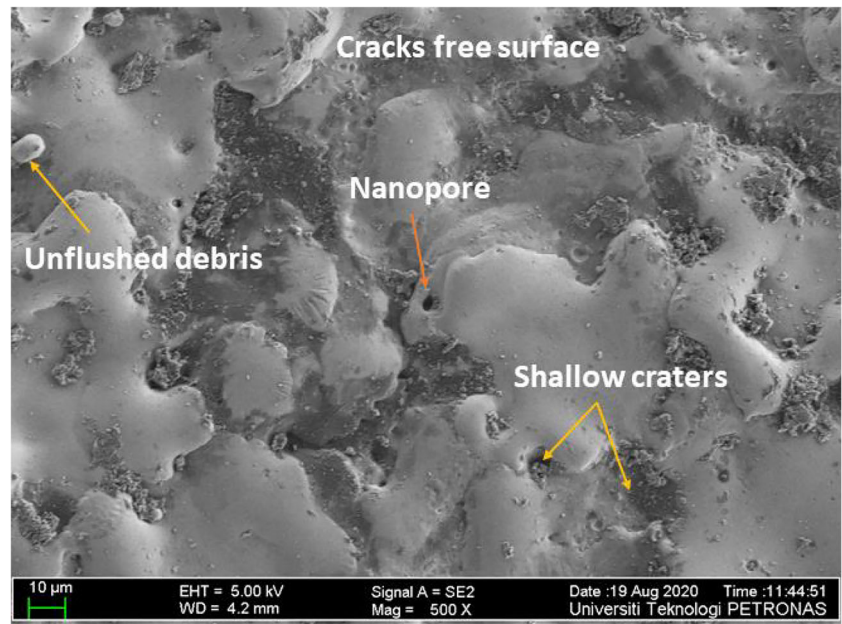


Fig. 14 Migration of elements on the machined specimen (EDX analysis)

Fig. 15 Surface morphology of the machined 316L steel (SEM analysis)



which improves the flushing performance and (b) scrubbing phenomena through the produced debris from the electrode, work part, and intermetallic products due to electromagnetic forces and turbulence effect in the machining gap [3, 4, 13, 35]. In this study, a comparatively thin recast layer is attained which may eliminate the further polishing process and improve the life span of the machined part. Because it is reported that a thick recast layer with high carbide contents may cause mechanical failure of the machined part because of increasing residual stresses, decreasing compression stress, and wear propagation in the formed substrates [3, 4, 11]. The surface morphology of the machined 316L steel is depicted in Fig. 15. In Fig. 15, a crack-free surface with nanopores, shallow craters, and unflushed debris is noticed. The obtained recast layer thickness at different

parameter settings is shown in Fig. 16a, b. From Fig. 16a, RLT of 11.85 μm is obtained at a peak current of 7 A, pulse-on time of 16 μs , MWCNT amount of 0.7 g/l, and duty cycle of 40%. In Fig. 16b, an RLT of 15.56 μm is measured corresponding to a 10-A peak current, 8- μs pulse-on time, 0.4-g/l MWCNT amount, and 40% duty cycle.

3.6 Optimal solutions for the machining performances

The responses such as SR and RLT improve when MRR increases based on the experimental points of view. In terms of the production point of view, MRR is chosen as “Greatest the better” while both SR and RLT are preferred as “Lowest the better”. Hence, finding the right combinations of the

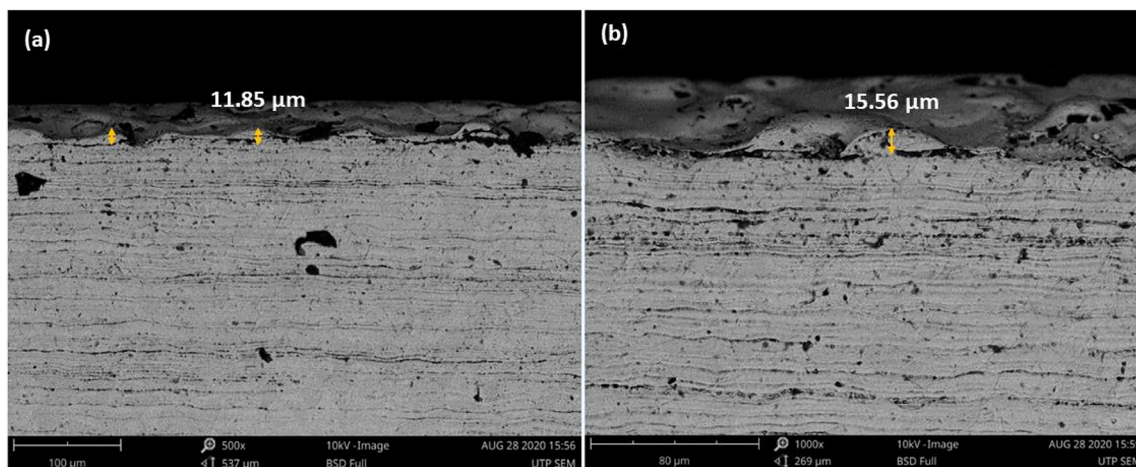


Fig. 16 The measured RLT at (a) peak current of 7 A, pulse-on time of 16 μs , MWCNT amount of 0.7 g/l, and duty cycle of 40% and (b) 10-A peak current, 8 μs pulse-on time, 0.4 g/l MWCNT amount, and 40% duty cycle

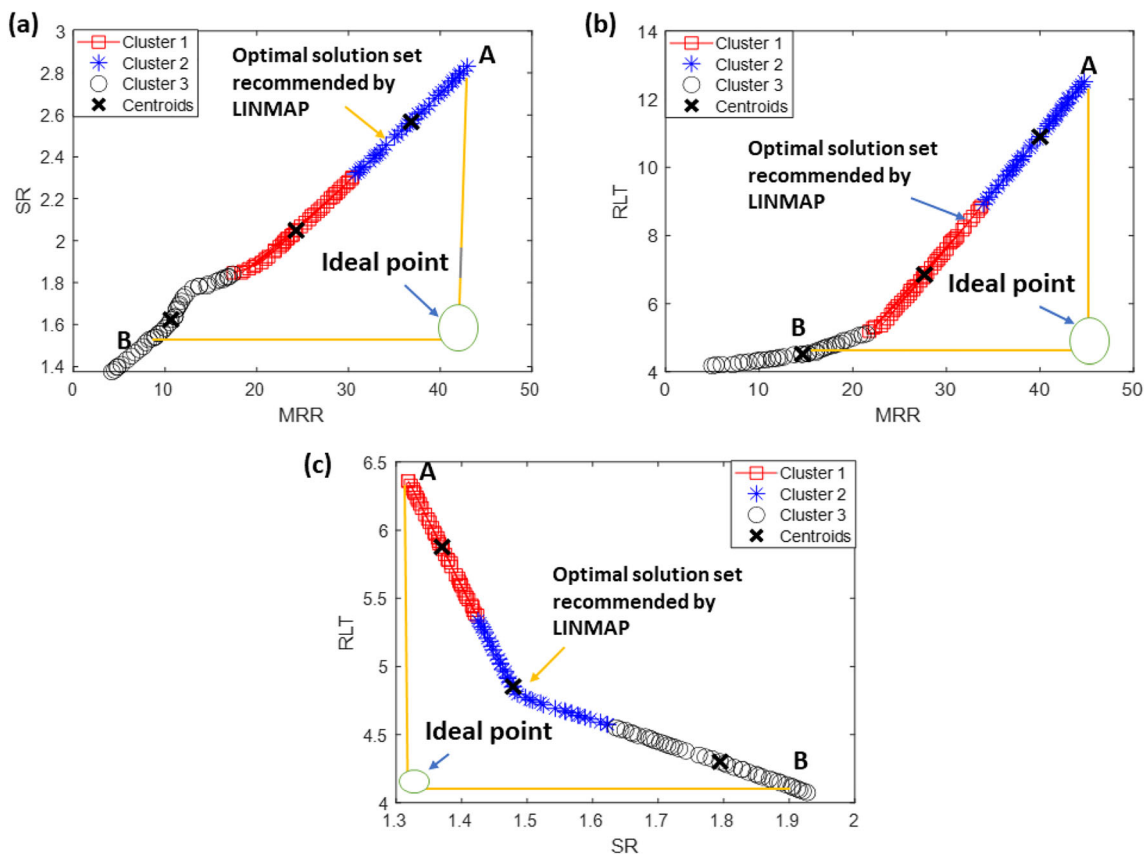


Fig. 17 Pareto optimal frontiers (a) SR vs MRR, (b) RLT vs MRR, and (c) RLT vs SR

associated factors that provide greater MRR with smaller both SR and RLT is very challenging. The following two objectives are proposed for this study.

$$\text{Objective}_1 = \text{Maximize}\{(\text{MRR})\}$$

$$\text{Objective}_2 = \text{Minimize}\{(\text{SR and RLT})\}$$

In total, 120 sets of the optimal solutions for each combination of the responses conforming the set objective functions were predicted through the NSGA-II technique. The Pareto

optimal frontiers representing the optimal solution sets are depicted in Fig. 17a–c. In this study, sorting of the best solution set was conducted through the LINMAP method following the ideal point sketched from two extreme points marked as A and B. Among 120 sets of the non-dominated solutions, the best 7 solution sets for each combination were selected with corresponding process factors that are included in Tables 5, 6, and 7. In addition to this, in total, 21 confirmatory experiments were carried out using the predicted combinations of the EDM process factors to evaluate the confidence

Table 5 Optimal solutions for maximizing MRR and minimizing SR with confirmation results

| Sl.no | A (A) | B (μs) | C (g/l) | D (%) | Predicted results | | Confirmatory results | | Error (%) | |
|-------|----------|------------|---------|-------|-------------------|------|----------------------|------|-----------|------|
| | | | | | MRR | SR | MRR | SR | MRR | SR |
| 1 | 5 | 8.4(~ 8) | 0.4 | 41 | 4.2 | 1.37 | 4.22 | 1.36 | 0.5 | 0.72 |
| 2 | 9.4(~ 9) | 15.7(~ 16) | 1 | 55 | 42.5 | 2.8 | 43.1 | 2.85 | 1.4 | 1.7 |
| 3 | 5.5 | 8.2(~ 8) | 0.41 | 53 | 9.95 | 1.58 | 9.23 | 1.49 | 7.2 | 5.69 |
| 4 | 5.5 | 8.2(~ 8) | 0.41 | 54 | 10.5 | 1.6 | 10.03 | 1.48 | 4.4 | 7.5 |
| 5 | 5 | 15.2 | 0.97 | 42 | 15.54 | 1.8 | 15.1 | 1.69 | 2.8 | 6.11 |
| 6 | 5.5 | 16 | 1 | 48 | 20.5 | 1.9 | 18.97 | 1.75 | 7.46 | 7.8 |
| 7 | 6 | 16 | 1 | 50 | 25.28 | 2.08 | 25.5 | 2.1 | 0.87 | 1 |

$$\text{Error} = \frac{\text{Abs}(\text{Predicted Results} - \text{Experimental results})}{\text{Predicted results}} \times 100\%$$

Table 6 Optimal solutions for maximizing MRR and minimizing RLT with confirmation results

| Sl.no | A (A) | B (μs) | C (g/l) | D (%) | Predicted results | | Confirmatory results | | Error (%) | |
|-------|-----------|--------------|---------|-------|-------------------|------|----------------------|------|-----------|------|
| | | | | | MRR | RLT | MRR | RLT | MRR | RLT |
| 1 | 5 | 8 | 0.9 | 55 | 4.96 | 4.1 | 5.3 | 4.33 | 6.85 | 5.6 |
| 2 | 9.8(~ 10) | 15.8(~ 16) | 1 | 55 | 44.73 | 12.5 | 45.43 | 12.8 | 1.56 | 2.4 |
| 3 | 5 | 10.4 | 1 | 55 | 10.27 | 4.34 | 9.76 | 4.28 | 4.9 | 1.38 |
| 4 | 5 | 12.8 | 1 | 55 | 15.28 | 4.53 | 14.97 | 4.6 | 2 | 1.5 |
| 5 | 5.3(~ 5) | 14.8(~ 14.4) | 1 | 55 | 20.7 | 5.07 | 18.88 | 4.87 | 8.7 | 3.9 |
| 6 | 6 | 16 | 1 | 55 | 25.47 | 6.1 | 24.67 | 6.2 | 3.1 | 1.6 |
| 7 | 7 | 16 | 1 | 55 | 30.39 | 7.78 | 28.86 | 7.25 | 5 | 6.8 |

Error = Abs (Predicted Results – Experimental results)/Predicted results × 100%

level of the predicted model. The confirmatory test result with experimental errors is reported in Tables 5, 6, and 7 as well. Since the optimal solution sets in Pareto frontiers generated through NSGA-II are the best non-dominated solutions, any set can be preferred according to the necessity of the manufacturers.

As shown in Fig. 17a, it is noticed that the responses reflect the contradictory essence according to the experimental point of view. SR shows an upward trend when MRR grows. Increment of MRR from 4 to 43 mg/min leads to an increase of SR from 1.3 to 2.9 μm. Hence, if MRR is deemed as the first priority, SR must be impaired due to conflict in nature. Based on the LINMAP approach, the optimal solution set for a combination of MRR and SR of 35.363 mg/min and 2.50 μm respectively is predicted with a corresponding peak current of 7.98 A, pulse-on time of 15.84 μs, MWCNT amount of 0.99 g/l, and duty cycle of 54.65%. From Table 5, the calculated confirmatory test errors are lower than 10% which ensure a high accuracy of the predicted solution sets for MRR and SR. run_1, run_2, and run_7 revealed lower errors for both the responses compared to the rest runs. The greatest MRR and SR of 43.1 mg/min and 2.85 μm respectively were obtained at a 9-A peak current, 16-μs pulse-on time, 1-g/l MWCNT

amount, and 55% duty cycle. However, the smallest MRR and SR of 4.22 mg/min and 1.36 μm respectively were estimated corresponding to a 5-A peak current, pulse-on time of 8 μs, MWCNT amount of 0.4 g/l, and duty cycle of 41%. The enclosed data with parentheses presented the predicted data with a machine-readable format which was employed to conduct the confirmatory experiments since the EDM machine could take the specific inputs. It is clearly shown that a MWCNT amount of 1 g/l was suggested for MRR of more than 10 mg/min while a 0.4-g/l MWCNT amount with low discharge energy was preferred for SR of lower than 1.48 μm. The best-fitted solution sets for minimizing SR and maximizing MRR can be chosen from solution_3 to solution_7.

As shown in Fig. 17b, it is noticed that the responses show a conflicting nature based on the experimental points of view. RLT reveals an upward trend with increasing MRR. Improving MRR from 5 to 45 mg/min leads to a rise of RLT from 4.1 to 12.5 μm. RLT increases gradually from 4.1 to 6 μm when MRR improves from 5 to 25 mg/min. According to the LINMAP technique, the best solution set for MRR and RLT of 29.67 mg/min and 7.48 μm respectively is predicted at a 6.74 peak current, 15.74-μs pulse-on time, 1-g/l MWCNT amount, and 54.76% duty cycle. From Table 6,

Table 7 Optimal solutions for minimizing both SR and RLT with confirmation results

| Sl. no. | A (A) | B (μs) | C (g/l) | D (%) | Predicted results | | Confirmatory results | | Error (%) | |
|---------|-------|--------|---------|-------|-------------------|------|----------------------|------|-----------|-----|
| | | | | | RLT | SR | RLT | SR | RLT | SR |
| 1 | 5 | 8 | 0.4 | 40 | 6.29 | 1.32 | 6.32 | 1.33 | 0.4 | 0.7 |
| 2 | 5 | 8 | 1 | 55 | 4.08 | 1.92 | 4.1 | 1.86 | 0.4 | 3.1 |
| 3 | 5 | 8 | 0.4 | 54 | 4.81 | 1.48 | 4.67 | 1.45 | 2.9 | 2 |
| 4 | 5 | 8 | 0.4 | 52 | 5.12 | 1.44 | 4.82 | 1.45 | 5.8 | 0.6 |
| 5 | 5 | 8 | 0.4 | 42 | 6.11 | 1.34 | 5.87 | 1.28 | 3.9 | 4.4 |
| 6 | 5 | 8 | 0.58 | 55 | 4.57 | 1.62 | 4.48 | 1.56 | 1.9 | 3.7 |
| 7 | 5 | 8 | 0.711 | 55 | 4.42 | 1.71 | 4.38 | 1.67 | 0.9 | 2.3 |

Error = Abs (Predicted Results – Experimental results)/Predicted results × 100%

the calculated errors for RLT and MRR are below 10% which confirm excellent predicted combination of the process factors for RLT and MRR. run_2, run_4, and run_6 revealed lower experimental errors compared to the rest runs. The smallest RLT and MRR of 4.33 μm and 5.3 mg/min respectively were measured at a peak current of 5 A, pulse-on time of 8 μs , MWCNT amount of 0.9 g/l, and duty cycle of 55%, whereas the largest RLT and MRR of 12.8 μm and 45.43 mg/min respectively were calculated at a peak current of 10 A, 16 μs pulse-on time, MWCNT amount of 1 g/l, and 55% duty cycle. It is concluded that large inputs of MWCNT amount, pulse-on time, duty cycle, and peak current were suggested for increasing both RLT and MRR. The best-fitted solution sets for minimizing RLT and maximizing MRR can be chosen from solution_1 to solution_7.

In Fig. 17c, RLT and SR show a reverse relation with each other according to the proposed objectives. A decline in RLT leads to a rise in SR. An augmentation of RLT from 4.1 to 6.4 μm leads to a reduction in SR from 1.93 to 1.32 μm . Based on the LINMAP approach, the best solution set for RLT and SR of 4.79 μm and 1.48 μm respectively is predicted corresponding to a peak current of 5 A, pulse-on time of 8.04 μs , MWCNT amount of 0.4 g/l, and duty cycle of 54.12%. From Table 7, the experimental errors for both RLT and SR are estimated below 10% which guarantee good predicted combination of the process variables for them. run_1, run_2, and run_7 provided lower experimental errors compared to the rest runs. The smallest RLT and the largest SR of 4.1 μm and 1.86 μm respectively were determined at a peak current of 5 A, pulse-on time of 8 μs , MWCNT amount of 1 g/l, and duty cycle of 55% while the greatest RLT and the lowest SR of 6.32 μm and 1.33 μm respectively were measured at a 5-A peak current, 8- μs pulse-on time, 0.4-g/l MWCNT amount, and 40% duty cycle. It is observed that a low MWCNT amount was suggested for increasing RLT and decreasing SR. The best fitted solution sets for minimizing both RLT and SR can be considered from the obtained solution_1 to solution_7.

4 Conclusion and suggestions

In this research, influences of the added MWCNT particles and the related process variables on the machining performances such as MRR, SR, and RLT while machining of 316L steel through the EDM method were explored. Through mathematical modeling, statistical, SEM, and EDX-based analyses, the following conclusions can be extracted:

1. Peak current, MWCNT amount, and pulse-on time are the momentous variables for MRR. Peak current is the most vital variable which contributes by 75.15% to MRR followed by MWCNT amount of 10.88% and pulse-on time of 10.47%. The largest MRR of 42.25 mg/min is calculated at a peak current of 10 A, MWCNT amount 1 g/l, duty cycle of 45%, and pulse-on time of 16 μs due the creation of more electrical discharges over a long time in the plasma channel and development of multiple electrical sparks around the machining gap by the single discharge. The obtained MRR shows comparatively higher than the results published in the previous studies.
2. All the related factors reveal significant for SR while duty cycle does not show any impact on RLT. Peak current is the most momentous variable for both SR and RLT followed by MWCNT amount, pulse-on time, and duty cycle. Peak current, MWCNT amount, duty cycle, and pulse-on time contribute to SR by 78.32%, 6.90%, 6.75%, and 7.53% respectively. In addition to this, peak current, pulse-on time, and MWCNT amount contribute to RLT by 77.84%, 7.25%, and 12.76% respectively. SR becomes large for high application of a peak current, pulse-on time, and MWCNT amount because of large craters formation on the surface machined by the single discharge. A high application of peak current and pulse-on time with low MWCNT amount and duty cycle causes a large RLT due to more debris production and deposition on the surface machined. The smallest both SR and RLT of 1.58 μm and 5.24 μm respectively are estimated corresponding to a 5-A peak current, 8- μs pulse-on time, 0.7-g/l MWCNT amount, and 45% duty cycle. The largest SR of 2.85 μm is obtained at a peak current of 10 A, MWCNT amount of 1 g/l, a duty cycle of 45%, and pulse-on time of 16 μs , but the highest RLT is measured at a 10-A peak current, 8- μs pulse-on time, 0.4-g/l CNT amount, and 40% duty cycle.
3. The best combinations of the process variables for the optimal responses based on the objective functions proposed have been obtained utilizing the NSGA-II technique. The best 120 solution sets for each combination of the performances have been predicted from which anyone can be preferred as per the requirement of the process engineers. The best-predicted solution set for acquiring large MRR and small SR is measured at a peak current of 6 A, pulse-on time of 16 μs , MWCNT amount of 1 g/l, and duty cycle of 50%. The required large MRR and low RLT have been predicted at a peak current of 6 A, pulse-on time of 16 μs , MWCNT amount of 1 g/l, and duty cycle of 55%. In addition to this, the optimal low both RLT and SR are achieved at a 5-A peak current, 8- μs pulse-on time, 0.4-g/l MWCNT amount, and 40% duty cycle. Among 120 sets of the optimal solution, the best 7 solution sets have been validated through conducting further confirmatory experiments. The confirmatory test errors are calculated less than 10% which guarantee a high accuracy of the prediction.

4. A thin recast layer with nanopores, shallow craters, and micro-crack free is observed through the SEM technique which may increase the durability of the 316L steel machined and avoid the post polishing process.

From this research work, an effective process is proposed to the audiences for fabricating the 316L steel with excellent machining and treated surface performances. A thin recast layer with low residual stresses and a micro-crack-free surface is ensured through SEM analysis which may avoid the mechanical failure of the 316L steel machined. The measured RLT is supposed to reduce further the polishing process. The predicted optimal solution sets may assist the process engineers conducting the experiments and process of 316L steel. However, this research work has acknowledged several limitations such as unstable machining due to applying more than 1 g/l of MWCNT concentration with a high applied voltage of more than 220 V, rapid dispersion of the heat energy by the highly conductive MWCNT mixed dielectric oil causing an interruption in MRR, presence of more carbides in the recast layer causing the wear propagation, and challenging to make separate the nano-, moderate-, and macro-sized pores formed using the profilometer. The aforesaid limitations should be addressed in future researches while machining 316L steel through the MWCNT-added EDM technique.

Acknowledgements Authors reveal their cordial gratefulness and admiration to Universiti Teknologi Petronas (UTP) for providing components and a working place.

Author contribution Idea and design of the study: Md Al-Amin, Ahmad Majdi Abdul-Rani; Conducting of experiments: Md Al-Amin; Data acquisition: Md Al-Amin, Rasel Ahmed, Muhammad Danial Bin Abd Rani, and Muhammad Umair Shahid; Analysis of data: Md Al-Amin, Rasel Ahmed, and Fatema Tuj Zohura.

Drafting the manuscript: Md Al-Amin, Fatema Tuj Zohura; Revision of the manuscript thoroughly for important intellectual content: Md Al-Amin, Ahmad Majdi Abdul-Rani, Muhammad Umair Shahid.

Approval of the manuscript for publication: Ahmad Majdi Abdul-Rani, Md Al-Amin, Fatema Tuj Zohura, Rasel Ahmed, Muhammad Umair Shahid, and Muhammad Danial Bin Abd Rani.

Funding The present research was fully assisted by the Ministry of Higher Education, Malaysia, through the FRGS fund-2020 (FRGS/1/2020/TK0/UTP/02/39; Cost center: 015MA0-132).

Data availability The authors have ensured 100% data transparency. All data generated or analyzed during this study are available in this research paper.

Code availability The authors customized the NSGA-II algorithms for optimization. Code is available as per request.

Declarations

Ethics approval Not Applicable

Consent to participate All authors have willingly participated in this publication.

Consent to publish The authors revised the manuscript critically and provided consent to publish.

Conflict of interest The authors declare no competing interests.

References

- Al-Amin M, Majdi AA-R, Rasel A, Rao TVVLN (2021) Multiple-objective optimization of hydroxyapatite-added EDM technique for processing of 316L-steel. *Mater Manuf Process* 36(4):1–14
- Abdel-Fattah TM, Lofus D, Mahapatro A (2011) Nanosized controlled surface pretreatment of bio metallic alloy 316L stainless steel. *J Biomed Nanotechnol* 7:794–800
- Al-Amin M, Majdi AA-R, Azeez AAA, Al'Hapis MAR, Hastuty S, Bryant MG (2020) Powder mixed-EDM for potential biomedical applications: a critical review. *Mater Manuf Process* 35(11):1789–1811
- Al-Amin M, Majdi AA-R, Danish M, Harvey MT, Azeez AAA, Hastuty S, Fatema TZ, Bryant MG, Rubaiee S, Rao TVVLN (2020) Assessment of PM-EDM cycle factors influence on machining responses and surface properties of biomaterials: a comprehensive review. *Precis Eng* 66:531–549
- Hanif M, Wasim A, Hakim AS, Sahar N, Sajid M, Nasir M (2019) Optimization of process parameters using graphene-based dielectric in electrical discharge machining of AISI D2 Steel. *Int J Adv Manuf Technol* 103:3735–3749
- Al-Amin M, Majdi AA-R, Azeez AAA, Bryant MG, Danish M, Azlan A (2020) Bio-ceramic coatings adhesion and roughness of biomaterials through PM-EDM: a comprehensive review. *Mater Manuf Process* 35(11):1157–1180
- Kunieda M, Lauwers B, Rajukar KP, Schumacher BM (2005) Advancing EDM through fundamental insight into the process. *CIRP Ann* 54:64–87
- Jadam T, Santosh KS, Saurav D, Masanta M (2020) Powder-mixed electro-discharge machining performance of Inconel 718: effect of concentration of multi-walled carbon nanotube added to the dielectric media. *Sadhana* 45:135
- Sachin M, Harmesh K (2017) Parametric optimization of multiwalled carbon nanotubes- assisted electrical discharge machining of Al-10%SiCp metal matrix composite by response surface methodology. *Mater Manuf Process* 32:263–273
- Rajeswari R, Shunmugam MS (2020) Finishing performance of die-sink EDM with ultrasonic vibration and powder addition through pulse train studies. *Mach Sci Technol* 24:245–273
- Sameehan SJ, Shrivana K, Harpreet SA, Sundeep M, Narendra BD (2015) Amorphous coatings and surfaces on structural materials. *Crit Rev Solid State Mater Sci* 41:1–24
- Azeez AAA, Majdi ABAR, Turnad LG, Prakash C, Eugen A, Al'Hapis MR, Sadaqat A (2017) A review of additive mixed-electric discharge machining: current status and future perspectives for surface modification of biomedical implants. *Adv Mater Sci Eng*:1–23
- Talla G, Gangopadhyay S, Biswas CK (2016) State of the art in powder mixed electric discharge machining: a review. *J Eng Manuf* 224(11):1725–1739 0(0):1-16
- Katsushi F, Hiromichi S, Masayuki S (2009) Influence of electrical conditions on performance of electrical discharge machining with powder suspended in working oil for titanium carbide deposition process. *Int J Adv Manuf Technol* 40:1093–1101

15. Kalyanmoy D, Amrit P, Sameer A, Meyarivan T (2002) A fast and elitist multiobjective genetic algorithm: NSGA-II. *IEEE Trans Evol Comput* 6(2):1–16
16. Yusoff Y, Nagadiman MS, Zain AM (2011) Overview of NSGA-II for optimizing machining process parameters. *Process Eng* 15: 3978–3983
17. Mitra K (2009) Multiobjective optimization of an industrial grinding operation under uncertainty. *Chem Eng Sci* 64(23):5043–5056
18. Seyed HRH, Shide SH, Edmundas KZ, Hadi A (2012) Extensions of LINMAP model for multi criteria decision making with grey numbers. *Technol Econ Dev Econ* 18(4):636–650
19. Yakup C, Fatih T (2020) An in-depth review of theory of the TOPSIS method: An experimental analysis. *J Manag Anal* 7(2): 281–300
20. Mai C, Hong H, Huang S (2012) Advantages of carbon nanotubes in electrical discharge machining. *Int J Adv Manuf Technol* 59: 111–117
21. Prabhu S, Vinayagan BK (2016) Optimization of carbon nanotubes based electrical discharge machining parameters using full factorial design and genetic algorithm. *Aust J Mech Eng* 14:161–173
22. Raymond M, Neeraj S, Kapil G, Paulo DJ (2019) Modeling and optimization of Wire-EDM parameters for machining of Ni55.8Ti shape memory alloy using hybrid approach of Taguchi and NSGA-II. *Int J Adv Manuf Technol* 102:1703–1717
23. Kamal K, Vijender S, Puneet K, Neeraj S (2019) EDM μ -drilling in Ti-6Al-7Nb: experimental investigation and optimization using NSGA-II. *Int J Adv Manuf Technol* 104:2727–2738
24. Emel K, Babur O (2013) Multi-objective optimization using Taguchi based grey relational analysis for micro-milling of Al 7075 material with ball nose end mill. *Measurement* 46:1849–1864
25. Eini S, Hamidreza S, Navid D, Moonyong L, Alireza B (2016) Multi-objective optimization of a cascade refrigeration system: exergetic, economic, environment, and inherent safety analysis. *Appl Therm Eng* 107:804–817
26. Kansal HK, Sehijpal S, Kumar P (2005) Parametric optimization of powder mixed electrical discharge machining by response surface methodology. *J Mater Process Technol* 169:427–436
27. Yubraj L, Gurpreet S, Amandeep SB, Prabin M, Purushottam K, Bikram T (2019) Surface modification of 316L SS with HAp nanoparticles using PM-EDM for enhanced biocompatibility. *Mater Today: Proceed* 15:336–343
28. Mohammadzadeh MS, Noordin MY, Brusa E (2013) Role of multi-walled carbon nanotubes on the main parameters of the electrical discharge machining (EDM) process. *Int J Adv Manuf Technol* 68: 1095–1102
29. Kamlesh P, Pramanik A, Chattopadhyaya S (2020) Machining performance of Inconel 718 using graphene nanofluid in EDM. *Mater Manuf Process* 35:3342
30. Kumar H (2014) Development of mirror like surface characteristics using nano powder mixed electric discharge machining (PMEDM). *Int J Adv Manuf Technol* 76:105–113
31. Kansal HK, Singh S, Kumar P (2007) Effect of silicon powder mixed EDM on machining rate of AISI D2 die steel. *J Manuf Process* 9:13–22
32. Pecas P, Henriques P (2003) Influence of silicon powder-mixed dielectric on conventional electrical discharge machining. *Int J Mach Tools Manuf* 43:1465–1471
33. Gurpreet S, Amandeep SB, Yubraj L, Prabin M, Purushottam K, Bikram T (2019) Machining performance and influence of process parameters on stainless steel 316L using die-sinker EDM with Cu tool. *Mater Today: Proceed* 18:2468–2476
34. Santosh K S, Saurav D (2018) Experimental studies on graphite powder-mixed electro-discharge machining of Inconel 718 super alloys: comparison with conventional electro-discharge machining. *J Process Mech Eng* 0(0): 1–19.
35. Tan PC, Yeo SH (2011) Investigation of recast layers generated by a powder-mixed dielectric micro electrical discharge machining process. *J Eng Manuf* 225:1051–1062

Publisher's note Springer Nature remains neutral with regard to jurisdictional claims in published maps and institutional affiliations.